Pressures on webs in wound rolls due to winding and contact

C. MOLLAMAHMUTOGLU, S. GANAPATHI, AND J.K. GOOD

ABSTRACT: Paper, film, and metallic webs have designed surfaces. Process engineers design these surfaces to ensure they will coat or print correctly. In some cases, such as tissue, the manufactured surface is designed to provide softness. After the web is formed, care must be taken to maintain the web surface for the intended use or for subsequent processing. Web surfaces can be damaged by contact pressure, which is due to multiple sources. Tissues can suffer decreased loft and softness as a result of excessive pressure. Winding webs into rolls creates pressure on each web layer that varies with radial location. Almost all high speed winders must employ a nip roller in contact with the outer surface of the winding roll to prevent air entrainment. The nip roller, which may or may not be covered with an elastomer, induces local dynamic pressures where it contacts the winding roll that travel at the surface velocity of the winding roll. After rolls are wound, they can witness additional surface contact pressure. Often rolls are stored on flat surfaces and the dead weight of the roll induces contact pressure. In other cases, the roll may be moved by a clamp truck that employs hydraulic pressure to clamp and lift the wound roll. The objective of this paper is to demonstrate a method by which the total pressure in a web due to winding and to contact can be determined. Wound rolls of newsprint and polyester will be subjected to compression tests to verify the method.

Application: This research can be applied to limit the pressure between wound rolls and contact surfaces to avoid damage of the web. Web surface damage and product loss can be mitigated by selecting winding and contact conditions that limit the total pressure witnessed by the web.

The development of pressure on webs due to winding is well known. Hakiel [1] developed the first robust winding model that allowed the prediction of contact pressure and circumferential stress as a function of radius in the wound roll. This model required inputs, including core outer radius and stiffness, winding tension as a function of radius, wound roll finish radius, web thickness, and material properties. The web material properties input included the radial and circumferential (MD) modulus of elasticity. The radial modulus was shown to be state dependent on contact pressure by Pfeiffer [2]. This required that Hakiel form a nonlinear solution since the model inputs were influenced by outputs. Hakiel was successful in developing and verifying his model via tests.

Almost all winding operations are performed in the presence of a nip roller. The nip roller limits the entrainment of air, helps maintain radial uniformity, and can increase the winding tension in the outer layer of a winding roll called the wound-on-tension (WOT). The WOT has components of web tension and nip-induced-tension (NIT). The NIT results from the nip roller inducing slippage in the outer layers of the winding roll. The development of the NIT is affected by contact pressures that result from the nip and complex slip stick behavior of web layers in the nip contact zone [3,4]. The nip induced stress field is dynamic and travels at the surface velocity of the winding roll. These dynamic stresses superimpose on the roll stresses that result from winding.

Rolls that have been wound are stored and transported in a variety of ways. Rolls can be stored supported by their cores, on their ends, and sometimes stacked, but can also be stored on their edges and, furthermore, in nested stacks. Rolls supported on edges will have static non-moving nip stress fields that will also superpose on the residual roll stresses due to winding. Similar static nip stress distributions will result when wound rolls are lifted by clamping their outer surface in preparation for transit.

The residual roll stresses due to winding [1-4] have been addressed. The total stress distributions resulting from winding, contact during winding, and contact during transit and storage are likely the largest stresses witnessed by the web and thus most likely to damage the web. These total pressures and stresses have not been addressed, and the objective of this paper is to develop a method to quantify them.

Analysis of the total stress field is complicated due, again, to the state dependency of the web material properties. Closed form expressions relating contact force to deformation and contact pressure are possible only if constant average material properties are assumed. Such expressions are intractable, as they force the user to assess what average radial modulus should be used, which depends on the contact pressure the expression was supposed to predict. Similar to the winding model of Hakiel [1], the only viable option is to employ computational tools and perform nonlinear analysis. The finite element method (FEM) is a robust and powerful solution technique for the analysis of such mechanical problems. Here, an FEM approach for the wound roll contact problem will be developed. In finite elements, the physical body is divided into sub-domains called "elements," and governing equations are defined on each of these elements in a discretized manner. These elements will allow the needed spatial variation of the material properties, which will be dependent on stresses due to winding and those due to contact [5,6].

A FINITE ELEMENT MODEL FOR WOUND ROLL CONTACT

Usually, the domain of contact will be small when compared to the domain size of the wound roll. For this application of the finite element method, we must break the domain into enough elements that the state dependency of the wound roll material properties are well characterized. We must also ensure there are sufficient elements in the region of contact to accurately model those deformations and internal stresses. This is best accomplished using a non-uniform mesh of elements.

A non-uniform mesh refinement

The contact problem is considered as a 2D plane strain problem taking advantage of symmetry and constraints as shown in **Fig. 1**. The boundaries are so remote from the contact they were assumed not to affect the solution of the problem. The form of the finite element discretization is shown in Fig. 1, with mesh refinement near the contact zone since the deformations, strains, and stresses are expected to vary rapidly there. The mesh refinement was based on use of geometric series in both the tangential and radial directions:

$$r_i = (r_{out} - r_{in})\left(\frac{k_r^{i-1} - 1}{k_r^{n_r} - 1}\right)^{p_r} + r_{in}, \quad i = 1,2,..,n_r \tag{1}$$

$$\theta_j = \frac{\pi}{2}\left(\frac{k_\theta^{j-1} - 1}{k_\theta^{n_\theta} - 1}\right)^{p_\theta}, \quad j = 1,2,..,n_\theta \tag{2}$$

where n_r and n_θ are the number of sectors along the radial and tangential directions, respectively. The parameters k and p are used to control the refinement in the r and θ directions. r_i and θ_j are the i^{th} radial position and the j^{th} tangential position in cylindrical coordinates. r_{out} and r_{in} are outer and inner radial boundaries of the region that is refined. In this case, r_{out} and r_{in} can be taken as roll outer radius and core outer radius, respectively; the core was not refined. An element's radial and tangential position will be used for identification:

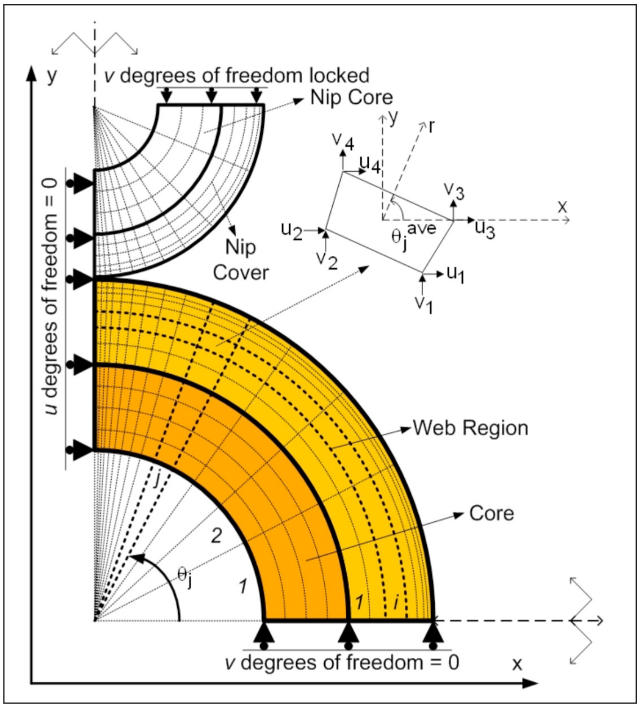

1. Finite element discretization of contact model for roll and nip.

$$e_{ID} = (i-1)n_\theta + j, \quad i = 1,2,..,n_r, \quad j = 1,2,..,n_\theta \tag{3}$$

Thus, e_{ID} becomes the identification number of an element per its radial and tangential location. The coordinates of the refined mesh can be used to define elemental coordinates. For a generic quadrilateral element, the elemental position vector in terms of the Cartesian coordinates of the 4 element nodes can be given as:

$$\begin{aligned} Q^{e_{ID}} = [&r_i\cos\theta_j \quad r_i\sin\theta_j \quad r_i\cos\theta_{j+1} \quad r_i\sin\theta_{j+1} \\ &r_{i+1}\cos\theta_j \quad r_{i+1}\sin\theta_j \quad r_{i+1}\cos\theta_{j+1} \quad r_{i+1}\sin\theta_{j+1}]^T \end{aligned} \tag{4}$$

This mesh refinement is also used for the nip roll cylinder when a non-rigid nip roll exists. In the case of a rigid nip, there is no need to model the nip roll per the contact algorithm.

The finite element formulation

The derivation begins with the approximation of continuous displacement field vector *U(x,y)* within the domain of an element:

$$U(x,y) = [u(x,y) \quad v(x,y)]^T \cong \Phi U^{e_{ID}} \tag{5}$$

$$\Phi = \begin{bmatrix} \phi_1 & 0 & \phi_2 & 0 & \phi_3 & 0 & \phi_4 & 0 \\ 0 & \phi_1 & 0 & \phi_2 & 0 & \phi_3 & 0 & \phi_4 \end{bmatrix}, \qquad U^{e_{ID}} = [u_1 \quad v_1 \quad u_2 \quad v_2 \quad u_3 \quad v_3 \quad u_4 \quad v_4]^T \tag{6}$$

where *u(x,y)*, *v(x,y)* are displacement fields in the x and y directions, respectively Φ; is the shape function matrix for a 4-node quadrilateral element; ϕ_i is the shape function associated with node I; and U^{eID} is the nodal displacement vector for the element. The components of the displacement vector are seen in Fig. 1. The strains are defined as:

$$\varepsilon^{e_{ID}} = DU(x,y) \cong (D\Phi)U^{e_{ID}} \tag{7}$$

$$\varepsilon^{e_{ID}} = \begin{bmatrix}\varepsilon_x & \varepsilon_x & \gamma_{xy}\end{bmatrix}^T, \quad D = \begin{bmatrix}\partial/\partial x & 0 & \partial/\partial y \\ 0 & \partial/\partial y & \partial/\partial x\end{bmatrix}^T \tag{8}$$

where ε_x, ε_y and γ_{xy} are the normal strains in the x, y directions and engineering shear strain, respectively. D is a differential operator matrix that operates only on the shape functions Φ. The stiffness matrix K^{eID} for an element is given as this expression:

$$K^{e_{ID}} = \int_{V^{e_{ID}}} B^T M^{e_{ID}}_{Cart.} B dV^{e_{ID}} \tag{9}$$

where $B = D\Phi$ is the strain-displacement matrix and M^{eID}_{Cart} is the element material matrix in Cartesian coordinates. The material orthotropic behavior for the wound roll elements are given with respect to cylindrical coordinates. The compliance matrix in cylindrical coordinates for plane strain orthotropic conditions is:

$$C^{e_{ID}}_{Cyl.} = \begin{bmatrix} 1/E_r - v_{rz}^2/E_z & -(v_{r\theta} + v_{rz}v_{z\theta})/E_\theta & 0 \\ -(v_{r\theta} + v_{rz}v_{z\theta})/E_\theta & (E_\theta - E_z v_{z\theta}^2)/E_\theta^2 & 0 \\ 0 & 0 & 1/G_{r\theta}\end{bmatrix} \tag{10}$$

$$M^{e_{ID}}_{Cyl.} = \left(C^{e_{ID}}_{Cyl.}\right)^{-1} \tag{11}$$

where E_r, E_θ, E_z , and $G_{r\theta}$ are the radial, tangential (MD) , axial (CMD), and shear moduli, and $\nu_{r\theta}$, ν_{rz}, and $\nu_{z\theta}$ are the Poisson ratios. Now, the element material matrix in Cartesian coordinates M^{eID}_{Cart} can be computed via an orthogonal transformation:

$$M^{e_{ID}}_{Cart.} = R^T M^{e_{ID}}_{Cyl.} R \tag{12}$$

$$R = \begin{bmatrix} \cos^2\theta_j^{ave} & \sin^2\theta_j^{ave} & \sin 2\theta_j^{ave} \\ \sin^2\theta_j^{ave} & \cos^2\theta_j^{ave} & -\sin 2\theta_j^{ave} \\ -\sin 2\theta_j^{ave}/2 & \sin 2\theta_j^{ave}/2 & \cos 2\theta_j^{ave}\end{bmatrix}, \tag{13}$$

$$\theta_j^{ave} = \left(\theta_j + \theta_{j+1}\right)/2$$

where R is the orthogonal transformation matrix and θ_j^{ave} is the element's orientation with respect to the x axis. The element stiffness matrix, Ex. (9), can be numerically calculated for all elements by using a master element concept. Assuming an isoparametric formulation, a transformation of coordinates from the actual *(x,y)* to natural *(η,ξ)* coordinates can be carried out:

$$X(x,y) = \begin{bmatrix}x(\eta,\xi) & y(\eta,\xi)\end{bmatrix}^T = \Phi Q^{e_{ID}} \tag{14}$$

where X is the position vector, Φ is the shape function matrix used in Ex. (5), and Q^{eID} is the elemental position vector defined in Ex. (4). The components of Φ for an isoparametric formulation of a quadrilateral element are:

$$\phi_1 = \frac{(1-\xi)(1-\eta)}{4}, \quad \phi_2 = \frac{(1-\xi)(1+\eta)}{4}, \quad \phi_3 = \frac{(1+\xi)(1-\eta)}{4}, \quad \phi_4 = \frac{(1+\xi)(1+\eta)}{4} \tag{15}$$

Using these shape functions, the stiffness integral (per unit width) is:

$$K^{e_{ID}} = \int_{-1}^{1}\int_{-1}^{1} \bar{B}^T M^{e_{ID}}_{Cyl.} \bar{B} \,|J|\, d\eta d\xi \tag{16}$$

where $\bar{B} = RB$ and $|J|$ is the determinant of the usual Jacobian matrix J of the transformation X. A 2x2 Gauss quadrature is employed to numerically integrate the stiffness integral (Ex. [16]). The finite element assembly procedure is used for all elements, which results in a total system stiffness matrix for the wound roll shown in Fig. 1.

The contact algorithm

This problem has two kinds of nonlinearity. The first type is material nonlinearity and stems from the known dependence of the radial modulus of elasticity of web materials on pressure or radial stress. A model which is often used for webs is:

$$E_r^{e_{ID}} = K_2\left(K_1 - \bar{\sigma}_r^{e_{ID}}\right) \tag{17}$$

where E_r^{eID}, $\bar{\sigma}_r^{eID}$ are radial modulus and average radial stress for the element e_{ID}. K_1 and K_2 are Pfeiffer's material parameters [2]. Prior to contact, there is an existing radial stress field, $\bar{\sigma}_r^{eID} = {}^0\bar{\sigma}_r^{eID}$, in the wound roll due to winding. A 1D nonlinear winding model, like that of Hakiel [1] but written for plane strain conditions, is employed to determine the stresses and the radial variation of the radial modulus due to winding. This radial modulus variation is used to set the initial radial modulus ${}^0E_r^{eID}$ for the elements prior to contacts.

The second type of nonlinearity is due to changes in geometry as the compression progresses. There is much information on computation of this type of nonlinearity [7]. A common approach is one of linearization using a tangent stiffness formulation based on the Newton-Raphson method. The current problem deals with the contact of cylinders in compression and involves smooth boundaries with predictable contact patterns. The contact will begin with zero contact force when the tip nodes of the cylinders barely contact, as was shown in Fig. 1. As the compression progresses, the nodes next to the tip node will sequentially come into contact. A simple quasi-linear approach based on node-to-node contact at the boundaries of the cylinders was employed. The material nonlinearity in this algorithm will be incorporated in a stepwise approach. In each step, an increment in deformation will occur as the compression progresses from one node to the next on the contact surfaces. Element material parameters will be taken as constant during a step deformation and updated at the end of the step. In this manner, the system will behave elastically during a step deformation. At the end of each step, the total elemental stresses will be updated by the increments in stress that resulted from the step deformation. The element material properties dependent on the total radial stress (Ex. [17]) are then updated.

In **Fig. 2**, geometry of contact of two cylinders is shown in detail. When seeking node-to-node contact, the corresponding nodes on the two cylindrical surfaces should be aligned in the lateral direction. The mesh refinement for the wound roll will dictate the lateral locations of the nodes on the boundary of the contacting surface, as shown in Fig. 1. Whether a nip is rigid or not, the boundary of the nip will be used to enforce appropriate contact conditions. The logic of the contact algorithm is similar for both cases. First, per Fig. 2, the initial gap size for the node i can be written:

$$\delta_i^0 = r_{out}\left(1-\sin\alpha_i\right)+r_{nip}\left(1-\sin\beta_i\right),\quad i=0,1,..,n_{cT} \tag{18}$$

where the angle α_i is directly dictated by the tangential refinement:

$$\alpha_i = \theta_{n_\theta+1-i} \tag{19}$$

The corresponding angle for the nip β_i can be easily calculated due to lateral alignment of the nodes to ensure node-to-node contact:

$$\beta_i = \arccos\left(\frac{r_{out}}{r_{nip}}\cos\alpha_i\right) \tag{20}$$

The superscript 0 of the gap size i, δ_i^0, in Ex. (18) identifies the compression step; 0 being the initial, 1 being the case when node 1 comes in contact, etc. n_{cT} is the total number of nodes allowed to contact and was set to $n_{cT} = n_\theta/2$.

The algorithm begins by applying a unit loading (F=½, due to symmetry) at the center of the nip, as shown in Fig. 1. The system is solved enforcing a set of boundary conditions. The symmetry boundary conditions along the vertical symmetry axis are enforced by setting the u degrees of freedom to zero. The wound roll is assumed to be rigidly supported (only the nip is moving), so the v degrees of freedom of the nodes along the bottom surface are set to zero. Nodes along the upper edge of the nip roll's quarter cylinder are forced to deform equally in the vertical (v) direction using multi-point constraint (MPC) equations. In step 1, the contact conditions on the boundary (non-slip, no penetration) begin with node 0 at the boundary of the wound roll and the corresponding node of the nip roll locked together in the x,y direction. The displacements of the wound roll due to the unit loading are shown in **Fig. 3** for nodes 0 and 1 as v^*_0 and v_1^{rw}, respectively. Due to the MPC enforced on node 0, the corresponding displacements for the nip are v^*_0 and v_1^{nip*}. These displacements will differ from their actual yet unknown counterparts, v_0, v_1^{wr}, v_1^{nip} which will just close the gap at node 1:

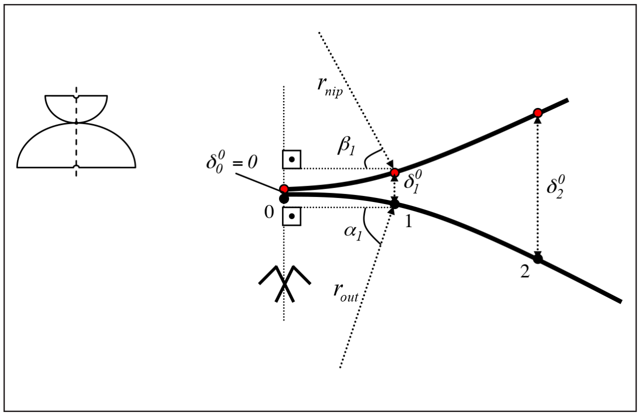

2. Initial geometry of contact of two cylinders.

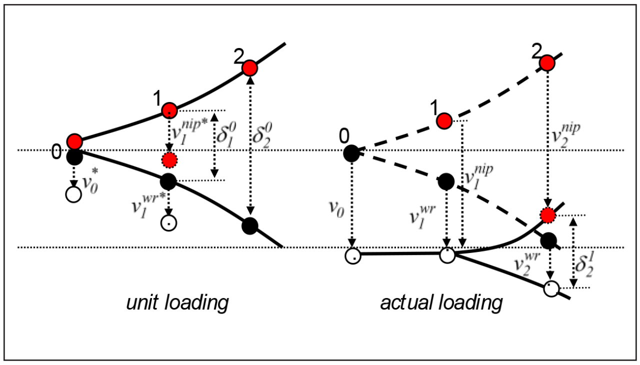

3. Deformations during step 1.

$$\delta_1^0 = v_1^{nip} - v_1^{wr} \tag{21}$$

Since linear elasticity is assumed within a step deformation, proportionality can be used to estimate deformations other than that due to a unit loading:

$$\frac{\Delta F_1/2}{1/2} = \frac{v_1^{wr}}{v_1^{wr*}} = \frac{v_1^{nip}}{v_1^{nip*}} \tag{22}$$

where ΔF_1 is the unknown actual incremental load that corresponds to actual displacements. Using the geometric compatibility condition from Ex. (21) and the proportionality condition from Ex. (22), a proportionality parameter κ_1 can be found to compute the unknown displacement field and the incremental load ΔF_1, which will just close the gap at node 1 for step 1:

$$\kappa_1 = \frac{\delta_1^0}{v_1^{nip*} - v_1^{wr*}} \tag{23}$$

$$U_1 = \kappa_1 U_1^*, \quad \Delta F_1 = \kappa_1 \tag{24}$$

where U_1 and U_1^* are global displacement vectors of the system for actual loading case and unit loading case for step 1. The gap sizes for step 2 are then updated:

$$\delta_i^1 = \delta_i^0 + v_i^{wr} - v_i^{nip}, \quad i = 2,3,..,n_{cT} \tag{25}$$

The incremental radial stresses for step 1, $\Delta^1\sigma_r^{eID}$ are calculated using the step 1 displacements U_1 and added to the radial stresses from winding. The updated pressures ${}^1\bar{\sigma}_r^{eID}$ are used to update the radial modulus of the elements for ${}^1E_r^{eID}$ step 1:

$$\begin{aligned} {}^1\bar{\sigma}_r^{eID} &= {}^0\bar{\sigma}_r^{eID} + \Delta\, {}^1\bar{\sigma}_r^{eID}, \\ {}^1E_r^{eID} &= K_2\left(K_1 - {}^1\bar{\sigma}_r^{eID}\right) \end{aligned} \tag{26}$$

This completes step 1. The same procedure is applied for steps 2,3,..,s by applying MPC for boundary node sets *(0,1),(0,1,2),..,(0,1,..,s-1)*, respectively, until the total load after step s surpasses the user defined nip load F_{nip} (force/ unit width):

$$\sum_{i=1}^{s} \Delta F_i \geq F_{nip} \tag{27}$$

The generalized algorithm is presented in **Table I**.

No.	Description
1	Use Hakiel's model to compute the initial winding stresses.
2	Generate refined mesh structure, extract initial values of element pressure from Hakiel's model and compute initial radial modulus: ${}^0E_r^{eID} = K_2\left(K_1 - {}^0\bar{\sigma}_r^{eID}\right)$
3	Set step number s=1, calculate initial gap sizes: $\delta_i^0 = r_{out}\left(1-\sin\alpha_i\right) + r_{nip}\left(1-\sin\beta_i\right)$, i=0,1,.., n_{cT}
4	Form system stiffness matrix for step s, apply boundary conditions via penalty method: $K_s = K_s\left({}^{s-1}E_r^{eID}\right)$
5	Apply MPC contact conditions for step s for boundary nodes i=0 to s-1.
6	Solve constrained system for unit vertical loading and obtain corresponding displacements U_s^*.
7	Use geometric compatibility and elastic proportionality to calculate proportionality factor for step s: $\kappa_s = \dfrac{\delta_s^{s-1}}{v_s^{nip*} - v_s^{wr*}}$
8	Obtain actual incremental compression force and deformations for step s and calculate incremental stresses: $\Delta F_s = \kappa_s\ U_s = \kappa_s U_s^*$
9	Update gap sizes, total pressures; recalculate pressure dependent radial modulus of elements: $\delta_i^s = \delta_i^{s-1} + v_i^{wr} - v_i^{nip}$, i=s+1 to n_{cT} ${}^s\bar{\sigma}_r^{eID} = {}^{s-1}\bar{\sigma}_r^{eID} + \Delta\, {}^s\bar{\sigma}_r^{eID}, {}^sE_r^{eID} = K_2\left(K_1 - {}^s\bar{\sigma}_r^{eID}\right)$
10	Check if target nip force is achieved or not: $\sum_{i=1}^{s} \Delta F_i \geq F_{nip}$ If yes, stop and output results, otherwise s=s+1 and go to 4.

I. Compression algorithm.

Material	PET	Newsprint	Geometrical	PET	Newsprint
K_1, KPa	7.24	0.145	Web thickness, mm	0.051	0.089
K_2	40.86	38.4	Roll width, cm	15.24	15.24
E_θ, MPa	4900	3896	Roll inner radius, cm	4.29	4.29
E_z, MPa	4900	3896	Roll outer radius, cm	11.99	11.99
$\nu_{r\theta}$, ν_{rz}	0.01	0.01	Core inner radius, cm	3.81	3.81
$\nu_{\theta z}$	0.3	0.3	n_r, n_θ	40	40
E_c, GPa	200	200	k_r, k_θ	0.95	0.95
ν_c	0.3	0.3	p_r, p_θ	0.5	0.5

II. Material and geometrical data for polyester (PET) film and newsprint.

NUMERICAL RESULTS AND EXPERIMENTAL VERIFICATION

Compression between rigid platens and determination of shear modulus

We will first study the load versus deformation of a wound roll compressed between flat, rigid platens. Both 51 µm (200 gage) polyester (PET) film and an 88 µm (350 gage) newsprint were modeled and tested. The material data is given in **Table II**.

These webs were wound with various tension levels and then compressed across their diameters between two rigid platens in an Instron 8502 servo-hydraulic testing system (Instron; Norwood, MA, USA). The experimental setup is shown in **Fig. 4**. The wound roll weight would interfere with the nip load levels and a counterbalance was used to eliminate the dead weight of the rolls from the contact. Thus the compression of the wound roll due to forces imposed by the testing system alone could be studied. During winding, pull tabs were inserted to verify the initial stresses computed from the winding code. The pull tabs were dislodged using a force gage from which the contact pressure could be estimated. In this context pressure, levels were measured inside wound rolls of PET film wound at two tension levels (T_w=*6.9* and *4.6* MPa), as shown in **Fig. 5**, with good agreement. Each test data point is the average from three windings. Similar results were found for the newsprint rolls.

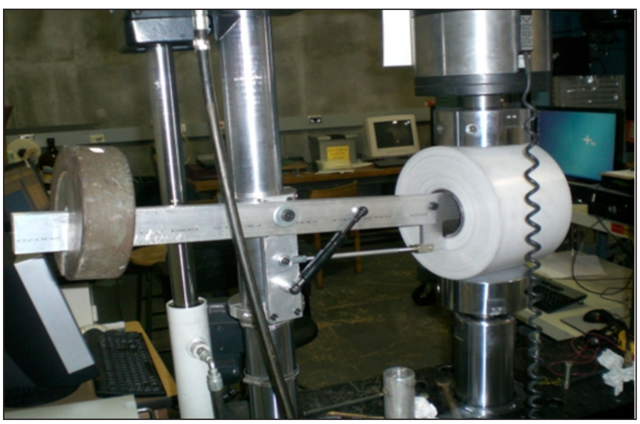

4. Experimental compression setup.

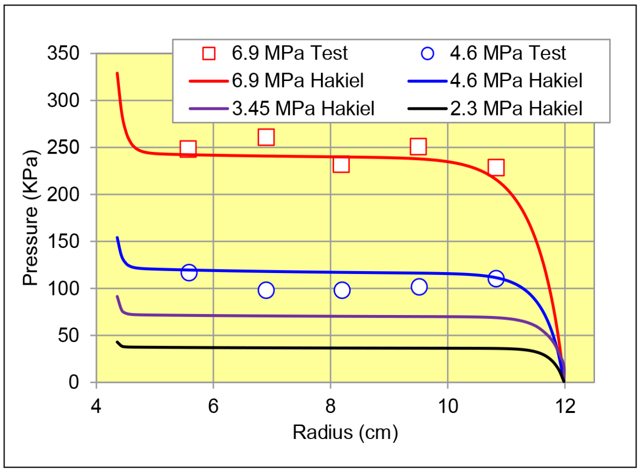

5. 51 µm PET film winding pressures from Hakiel's winding model and tests as a function of winding tension.

The compression model requires an input for the shear modulus $G_{r\theta}$ (Ex. [10]). $G_{r\theta}$ significantly affects the results of the compression model. There is no information in the literature on the prediction of $G_{r\theta}$ for stacks of web material. It is generally accepted that $G_{r\theta}$ is an independent constant for orthotropic materials. For bulk orthotropic materials, two relations were found, Szilard [8] and Cheng [9]:

$$G_{r\theta}^{\mathrm{Szilard}} = \frac{\sqrt{E_r E_\theta}}{2\left(1+\sqrt{v_{r\theta} v_{\theta r}}\right)} \tag{28}$$

$$G_{r\theta}^{\mathrm{Cheng}} = \frac{E_r E_\theta}{E_r\left(1+v_{\theta r}\right)+E_\theta\left(1+v_{r\theta}\right)} \tag{29}$$

For web materials, the out-of-plane Poisson's ratios are small

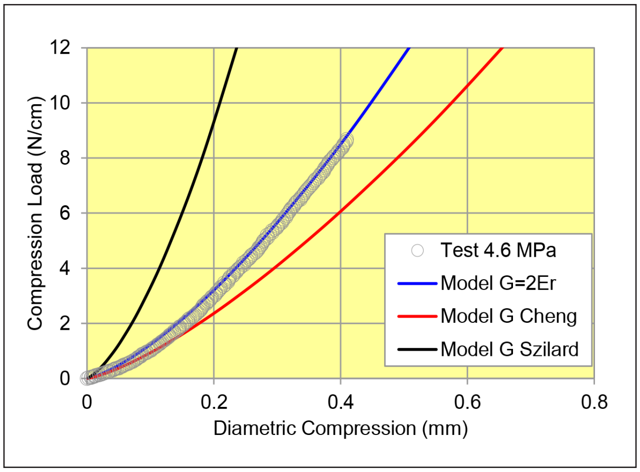

6. Comparison of shear modulus expressions used in contact analysis when winding 51 µm PET film at 4.6 MPa winding tension.

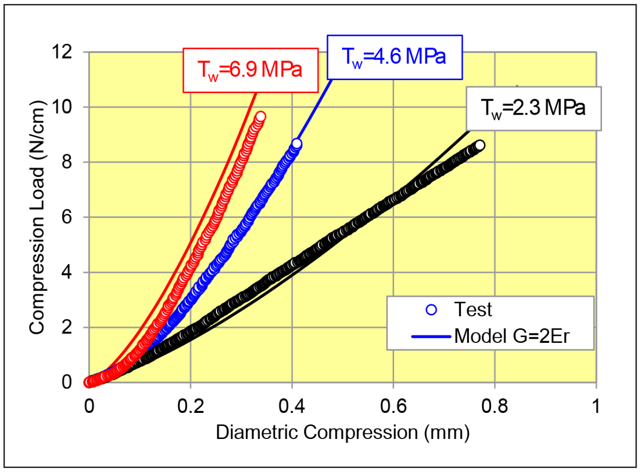

7. Model and test comparisons for PET film wound at various winding tensions.

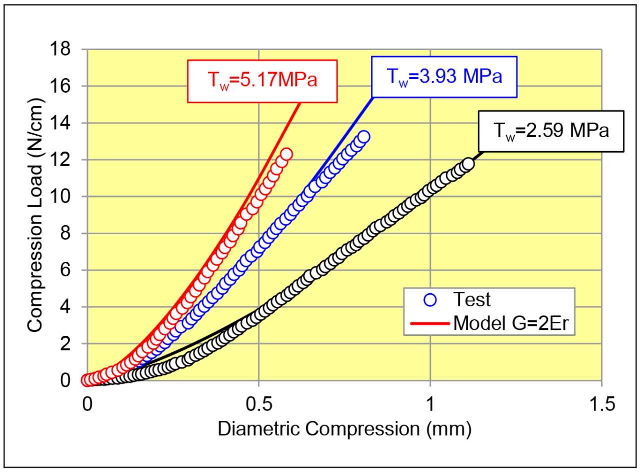

8. Model and test comparisons for newsprint.

when compared to unity ($\nu_{r\theta}$, $\nu_{r\theta} \ll 1$). Also, the tangential modulus is far greater than the radial modulus ($E_\theta \gg E_r$). Thus, the expressions of Szilard (Ex. [28]) and Cheng (Ex. [29]) reduce:

$$G_{r\theta}^{\text{Szilard}} \approx \frac{\sqrt{E_r E_\theta}}{2} \quad (30)$$

$$G_{r\theta}^{\text{Cheng}} \approx E_r \quad (31)$$

Both expressions involve the radial modulus E_r and the shear modulus also becomes pressure dependent. The load-deformation curves for the PET film wound at $T_w=4.6$ MPa are shown in **Fig. 6**. The compression model produced quite different results using the original forms of shear modulus, Ex. (30) and Ex. (31). Twice, the value of the shear modulus due to Cheng ($G_{r\theta}=2G_{r\theta}^{Cheng} \approx 2E_r$) produced good agreement with the test data. To verify this expression, $G_{r\theta} = 2E_r$ was employed in the compression model for other winding tension levels and on newsprint. Load versus deformation results are shown in **Figs. 7** and **8** from model and tests for various winding tensions for the PET film and newsprint, with good agreement in all cases. Thus, this combined procedure (experiment and numerical model) verifies the use of this relation for two very different materials under various winding conditions.

Modeling of rubber covered rollers

In many winding applications, nip rollers are covered with a deformable layer often composed of rubber. Rubber is known for its complexity in modeling [10,11]. Rubber is often characterized in the field by a handheld measurement of hardness (Shore A or International Rubber Hardness Degrees [IRHD]). Here, hardness will be used to characterize the rubber properties. This was adopted from an earlier work that modeled the nip contact between rubber covered nip rollers in contact with other rubber covered and uncovered rollers [12]. One portion of this study involved extensive compression tests in which the modulus of elasticity (E_{rubber}) and Poisson's ratio (ν_{rubber}) were measured for various rubber types (carboxilated nitrile, ethylene propylene, hypalon, natural, neoprene, nitrile, and urethane) and various hardness levels. An exponential expression was found to nicely fit the modulus for all rubber types as a function of hardness (IRHD) alone:

$$E_{\text{rubber}} = 0.1446 e^{0.0564 * \text{IRHD}} (\text{MPa}) \quad (32)$$

The experimental values for Poisson's ratio for various rubbers yielded an average value of 0.459. Here, the rubber cover will be modeled using the quadrilateral elements described earlier, but with isotropic properties per Ex. (32) and the stated Poisson's ratio. The efficacy of modeling rubber covered rollers in this way has already been verified [12] and will be incorporated into contact analysis with wound rolls.

	Rigid Surface	Rigid Roller	Soft Rubber Covered	Hard Rubber Covered
IRHD	-		40	80
Cover thickness, cm	-		1.27	
Nip roller diameter, cm	40.64			
Wound roll inner diameter, cm	8.38			
Wound roll outer diameter, cm	60.96			
Wound roll width, cm	60.96			
T_w, MPa	3.45			
Nip load, N/cm	36			

III. Material and geometrical data for compression scenarios.

Some compression scenarios and altered stress states

In this section, the contact stresses between wound rolls and various contact surfaces will be examined. The scenarios include compression of a wound roll by hard (IRHD 80) and soft (IRHD 40) rubber covered rollers, a rigid roller, and, finally, compression due to contact with a rigid flat surface. The material and geometric data for the rollers are given in **Table III**. The selected web material is the polyester film that was defined in Table II and previously used in the diametric compression tests. In this case, the PET film was wound with a tension level of 3.45 MPa and the internal pressure due to winding alone is shown in Fig. 5. The nip load was selected to be 36 N/cm for all scenarios. The compression algorithm is of the displacement control type. A solution completes once the load level in a step exceeds the user defined value (Step

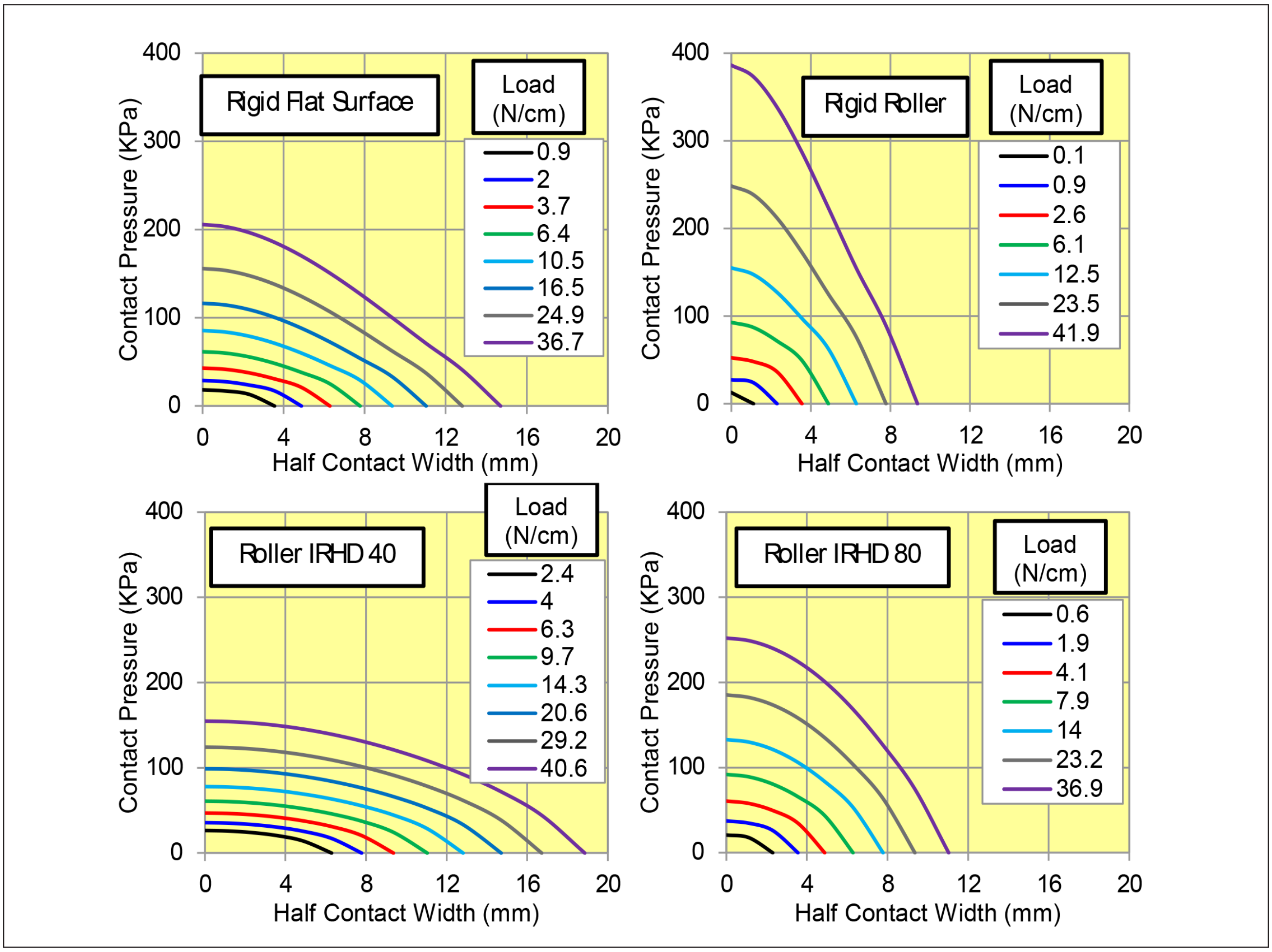

9. Surface contact pressures for polyester wound rolls.

10, Table I). The final nip load level will differ slightly from the 36 N/cm due to the different contact scenarios.

In **Fig. 9**, the surface contact pressures with respect to half contact width are shown. First, compare the results between the rigid flat surface and the rigid roller. Note how the curvature of the rigid roller surface has almost doubled the contact pressure when compared to the rigid flat surface. Next, compare the results from the three roller contact scenarios. As might be expected, the contact pressures are highest for the rigid roller. In comparison, the rollers with the IRHD 80 and 40 covers successively produce less contact pressure but greater contact width, respectively. Thus, it is evident that the compression algorithm developed could be used to produce nip cover designs that would limit the contact pressure. The average pressure in the roll due to winding is 71 KPa (Fig. 5). From Fig. 9, it becomes obvious that the contact pressures can be much greater than the pressure due to winding and should be considered when web quality is sensitive to pressure. The maximum nip load of 36 N/cm was arrived at by calculating the dead weight of the wound roll of polyester resting on a rigid flat surface; thus, these are not unreasonable contact loadings.

CONCLUSIONS

The model developed here can be used to address the total stress state of a wound roll in contact with storage surfaces or with rigid or rubber covered nip rollers. Significant pressures were shown to develop in the contact zone when compared to the pressure due to winding alone. The model produced results that show that harder nip surfaces produce higher contact pressures for given nip loads. This is intuitive, but the model has gone further to quantify the contact pressure produced by a nip roller of a given diameter, cover thickness, and cover hardness. From off line tests, the pressures that damage

ABOUT THE AUTHORS

We chose to research this topic because webs and wound rolls are often damaged by contact pressure, but no method could be found in the literature to predict the contact pressure. Closed form expressions for contact pressure exist, but they are limited for use on isotropic materials with constant elastic modulus. Wound rolls are extremely anisotropic and the radial elastic modulus is not constant due to state dependency on pressure.

We have much experience in the use and development of winding models, which were a prerequisite to the development of a model that can predict contact pressure. One of the outputs of winding models is the internal roll pressure as a function of radius, which then makes the radial modulus of elasticity known, also as a function of radius. This provides the starting point for any contact analysis of the wound roll by nips or support surfaces.

The most difficult aspect of this research was addressing the geometric and material nonlinearity in the contact model. This was addressed by the continual update of geometry and material properties with increased nip load and contact area. Our most interesting finding was that the results show how important nip roller design (diameter, cover stiffness, etc.) can be in controlling the contact pressure.

When web damage due to contact pressure is a problem, mills should ensure that those responsible are accounting for web properties, winding stresses, nip loads, and nip properties when proposing solutions. Nip loads, nip properties, and winding stresses can all be controlled to limit contact pressure. It is not unusual for the hardness of a nip cover to increase with age in the process environment and require periodic replacement. Models such as the one described here can be used to quantify cover hardness bounds for maintenance to prevent web damage due to contact pressure.

Mollamahmutoglu

Ganapathi

Good

Our goal at the Web Handling Research Center is to address all aspects of improving wound roll quality. The method developed in this publication addresses steady state contact stresses between a wound roll and a contact surface. Few winding rolls and nip rolls are concentrically perfect, which produces vibration in the winder and dynamic components of nip loads and contact pressures. A next step would be to investigate how these dynamic components of contact pressure compare in magnitude to the steady state pressures computed by the method described here. In the extreme, roll vibration can be so severe that wound rolls are thrown from winders. In less extreme cases, winder vibration can be responsible for dynamic contact pressures that result in web quality loss.

Mollamahmutoglu is assistant professor, Civil Engineering, at Yildiz Technical University, Davutpasa Campus in Istanbul, Turkey. Ganapathi is certification engineer II at Recaro Aircraft Seating Americas in Northlake, TX, USA. Good is professor and Noble Foundation chair, Mechanical & Aerospace Engineering, at Oklahoma State University in Stillwater, OK, USA. Email Good at james.k.good@okstate.edu.

webs can be quantified. Using tools such as the model described here, we can ensure the web never experiences damaging pressure levels by designing the contact surfaces and limiting the contact loads. One of the indirect findings that may have value to others was the development of a relation between the radial and the shear modulus of the wound roll. The model developed will support making good decisions on roll storage. Decisions regarding whether rolls are to be stored on flat surfaces or cradles and if nesting will be allowed can be made knowing the impact on contact pressure and web quality. **TJ**

ACKNOWLEDGEMENTS

The authors would like to acknowledge the sponsors of the Web Handling Research Center of Oklahoma State University in Stillwater, OK, USA, for the support they provided, which allowed us to pursue the research reported here.

LITERATURE CITED

1. Hakiel, Z., *Tappi J.* 70(5): (113)1987.
2. Pfeiffer, J.D., *Tappi* 49(8): 342(1966).
3. Kandadai, B.K. and Good, J.K., *TAPPI J.* 10(6): 25(2011).
4. Good, J.K., Kandadai, B.K., and Markum, R., *J. Pulp Pap. Sci.* 35(1): 17(2009).
5. Johnson, K.L., *Contact Mechanics*, Cambridge University Press, Cambridge, UK, 1989, pp. 139-140.
6. Bathe, K.J., *Finite Element Procedures*, Prentice Hall, Upper Saddle River, NJ, USA, 1996, p. 485.
7. Wriggers, P., *Computational Contact Mechanics*, John Wiley & Sons, Hoboken, NJ, USA, 2002.
8. Szilard, R., *Theory and Analysis of Plates*, Prentice Hall, Upper Saddle River, 1974, pp. 375-376.
9. Cheng, S. and Cheng, C.C. in *Mechanics of Wood and Paper Materials*, American Society of Mechanical Engineers, AMD-Vol. 112, MD-Vol. 23, 1990, pp. 63-65.
10. Boast, D. and Coveney, V.A., *Finite Element Analysis of Elastomers*, John Wiley & Sons, Hoboken, 1998.
11. Miller, R.D.W., Br. *J. Appl. Phys.* 15(11): 1423(1964).
12. Good, J.K., "Modeling Rubber Covered Nip Rollers in Web Lines," *Int. Conf. Web Handling, 6th*, Oklahoma State University, Stillwater, OK, USA, June 2001, pp. 159-186.